Antarctic Bottom Water Warming Between the 1990s and the 2000s: Contributions to Global Heat and Sea Level Rise Budgets*

Sarah G. Purkey[1,2] and Gregory C. Johnson[2,1]

[1]*School of Oceanography, University of Washington, Seattle WA 98195, USA*

[2]*NOAA/Pacific Marine Environmental Laboratory, Seattle WA 98115, USA*

for *Journal of Climate*

Submitted 16 February 2010

---

*Pacific Marine Environmental Laboratory Contribution Number 3524.

Corresponding author address: Gregory C. Johnson, NOAA/Pacific Marine Environmental Laboratory, 7600 Sand Point Way N.E., Bldg 3, Seattle, WA 98115. E-mail: gregory.c.johnson@noaa.gov.

ABSTRACT

We quantify global abyssal and deep Southern Ocean temperature trends since the 1990s to assess the role of recent warming of abyssal and deep Antarctic waters in global heat and sea level budgets. We compute warming rates with uncertainties along 26 full-depth, high-quality hydrographic sections that have been occupied two or more times between 1980 and the present. We divide the globe into 32 deep basins defined by the topography and climatological ocean bottom temperatures and estimate deep temperature trends in all sampled basins. The three southernmost basins show a strong statistically significant abyssal warming trend, with that warming signal weakening to the north in the central Pacific, western Atlantic, and eastern Indian Oceans. Eastern Atlantic and western Indian Ocean basins show statistically insignificant abyssal cooling trends. Excepting the Arctic Ocean and Nordic seas, the global ocean heat content change below 4000 m since the 1990s is equivalent to a heat flux of 0.024 (±0.010) W m^{-2} over the entire surface of the earth. Deep (1000–4000 m) warming of waters mostly of Antarctic origin south of the Sub-Antarctic Front of the Antarctic Circumpolar Current adds 0.065 (±0.063) W m^{-2}. The warming below 4000 m produces a 0.047 (±0.020) mm yr^{-1} increase in global average sea level and the deep warming south of the Sub-Antarctic Front adds another 0.087 (±0.083) mm yr^{-1}. These results suggest that deep and abyssal warming of Antarctic origin accounts for substantial fractions of the present global energy and sea level budgets.

1. Introduction

A warming climate is unequivocal, with the global top of the atmosphere radiative imbalance currently on the order of one W m^{-2}, very likely due to anthropogenic greenhouse gasses (Solomon et al. 2007). Over the past few decades, about 80% of the energy resulting from this imbalance has gone into heating the oceans (Levitus et al. 2005), which have a large heat capacity compared with the land or the atmosphere. This warming is important in both Sea Level Rise (SLR) and in climate projections (Bindoff et al. 2007).

The Earth's radiative imbalance affects SLR in two ways (e.g., Cazanave et al. 2008; Trenberth and Fasullo 2009). Much of the heat raises ocean temperature, causing thermal expansion, termed thermosteric SLR. A much smaller portion of the heat acts to melt continental ice, adding mass to the ocean, termed eustatic SLR. Highly accurate satellite measurements from TOPEX/Poseidon and Jason altimetry have reported an average rate of SLR of 3.1 mm yr^{-1} between 1993 and 2003, with roughly half of that being due to thermal expansion, and half due to mass changes, mostly from melting of continental ice (Bindoff et al. 2007). However, there is still debate over the exact breakdown of SLR between eustatic and steric components. Some recent SLR budgets using observations of upper ocean warming and mass changes either do not close or have high uncertainty (Miller and Douglas 2004; Raper and Braithwaite 2006), especially post-2003 (Willis et al. 2008). Other SLR and global energy budgets rely on poorly constrained deep ocean heat uptake for closure (Domingues et al. 2008; Murphy et al. 2009).

Models contain a delay between greenhouse gas forcing and ocean heat uptake because of the long equilibration time of the ocean (Hansen et al. 2005). Therefore, even if we stopped producing greenhouse gases, ocean temperatures and sea level would continue to rise for centuries. Furthermore, model fluxes of heat from the ocean surface layers to the deep ocean differ dramatically depending on model details. This climate sensitivity affects predictions of the magnitudes and rates of future sea level rise and global atmospheric warming (Raper et al. 2002; Meehl et al. 2005). Indeed, uncertainty involved in deep-ocean heat uptake may be the largest cause of variation among climate projections (Boe et al. 2009), making it vital to close observed heat and sea level rise budgets, including the deep ocean, for the purposes of adequately constraining predictions of and preparing for future climate change.

The deep ocean is ventilated by dense water sinking at high latitudes. North Atlantic Deep Water (NADW) is a mixture of water masses formed through deep convection processes in the Nordic and Labrador Seas (LeBel et al. 2008). Antarctic Bottom Water (AABW) is formed by a complex interaction of water masses and physical processes, with varieties produced in at least three source regions: The Weddell Sea, the Ross Sea, and the Adelie Coast (Orsi et al. 1999). While pure AABW is confined to the Southern Ocean, here we will refer to abyssal waters primarily of Antarctic origin as AABW for simplicity.

NADW and AABW feed the deep and abyssal limbs of the global ocean Meridional Overturning Circulation (MOC; Lumpkin and Speer 2007). NADW dominates the water column from intermediate depths to the bottom in the North Atlantic, although a small contribution from AABW can still be found there in the abyss (Johnson 2008). In the

western South Atlantic, a significant layer dominated by AABW spreads northward under the NADW. In the Pacific and Indian Oceans, however, the deep and abyssal regions are dominated by AABW with only a small fraction of NADW present (Johnson 2008).

Recent studies have revealed property changes in AABW near their source regions. In the Weddell Sea, the deep water has warmed at a rate of 0.009 °C yr^{-1} between 1990 and 1998, followed by a period of cooling (Fahrbach et al. 2004). In the Ross Sea, shelf and surface water has freshened and warmed at mid-depths (190–440 m) and in the deep layer within the Gyre (Jacobs et al. 2002; Ozaki et al. 2009). Deep water off the Adelie coast along 140°E has also shown cooling and freshening on isopycnals (Aoki et al. 2005; Rintoul 2007; Johnson et al. 2008a).

Warming of AABW is not limited to the Southern Ocean. In the deep basins north of the Antarctic Circumpolar Current (ACC), AABW has also shown signs of warming, although at a reduced rate compared with that nearer its sources. In the Atlantic Ocean, the deep water in the Scotia Sea, Argentine Basin, and Brazil Basin — all fed by AABW originating from Weddell Sea — has warmed over the past two decades (Coles et al. 1996; Johnson and Doney 2006; Zenk and Morozov 2007; Meredith et al. 2008). These changes, as well as circulation changes in North Atlantic (Johnson et al. 2008a) and North Pacific (Kouketsu et al. 2009) Oceans, may be influenced by a reduction in density or formation rates of AABW. In the eastern Indian Ocean warming has been observed in the Australian Antarctic Basin but little change has been seen to the north (Johnson et al. 2008b). Finally, the abyssal Southwest and Central Pacific Basins have both significantly and widely warmed over the past two decades (Fukasawa et al. 2004; Kawano et al. 2006; Johnson et al. 2007).

Furthermore, the upper water column throughout much of the Southern Ocean has also warmed over the last few decades, apparently at a faster rate than the upper ocean global mean (Gille 2002; 2008; Böning et al. 2008). This warming has been attributed to an intensification of the Southern Ocean westerly winds as well as changes in surface buoyancy (heat and freshwater) fluxes (Gille 2008; Böning et al. 2008).

High-quality temperature observations of the global deep ocean originate mostly from ship-based Conductivity-Temperature-Depth (CTD) instruments. The international World Ocean Circulation Experiment (WOCE) Hydrographic Programme accomplished a full-depth high-resolution high-accuracy hydrographic survey of the global ocean in the 1990s, with coast-to-coast zonal and meridional sections crossing all major ocean basins. A key subset of these sections are being reoccupied in support of the Climate Variability (CLIVAR) and carbon cycle science programs, now coordinated by the international Global Ocean Ship-based Hydrographic Investigations Program (GO-SHIP), providing a means for studying decadal timescale changes in the deep ocean.

Here data from all the WOCE hydrographic sections that have been repeated and those repeats are used to estimate the heat uptake by AABW since the early 1990s. We describe the data along with the initial gridding and screening methodologies in Section 2. In Section 3, we estimate rates of change in the temperature with time for the 32 deep ocean basins (excluding the Arctic Ocean and Nordic Seas) and in the Southern Ocean up to intermediate levels. We then use these rates to estimate local and global contributions to the heat and sea level rise budgets from AABW warming from the 1990s into the 2000s in Section 4. We conclude with a discussion of the results in Section 5.

2. Data

The data set used for this study is an aggregate of 26 full-depth, high-quality hydrographic sections that have been occupied two or more times between 1981 and 2009 (Figs. 1–2). Throughout this study sections are referred to by their WOCE Hydrographic Programme designated IDs (Figs. 1–2). The first occupation of most sections was in the 1990s during WOCE, with subsequent occupations, mostly during the 2000s, in support of the CLIVAR and Carbon Cycle Science Programs (Fig. 3). The six sections with occupations prior to 1990 were sampled during the ramp-up to WOCE with the earliest occupation considered here being the 1981 occupation of A05. The most recent occupation included in this study is one of I05, completed in spring 2009.

Sections have a minimum of at least one occupation during WOCE followed by a second occupation 6–12 years later, with the exception of A01, A02, and P03 (Fig. 3). Both A01 and A02 have multiple occupations in the 1990s but data from subsequent occupations were not readily available. P03 was occupied in 1985 and 2005/6 but has no occupations in the 1990s. The shortest time interval between the first and last occupation of a section is 3 years, for A02, from 1994 to 1997; and the longest time interval is 22 years, for A05 from 1981 to 2004. The mean and median time differences between first and last occupations for repeat sections are 12.8 and 11.4 years. All occupations of the sections that were publicly available from http://cchdo.uscd.edu as of December 2009 are considered here.

Data collected along each section are highly accurate and well sampled in the vertical and horizontal. Vertical profiles of temperature, conductivity, and pressure were collected at each station from the surface to a depth of 10–20 m from the bottom using a

CTD. Horizontal station spacing was nominally 55 km, often less over rapidly changing bathymetry. Salinity was calculated from CTD conductivity, temperature, and pressure data and calibrated to bottle samples standardized with International Association for the Physical Science of the Oceans (IAPSO) Standard Seawater using the 1978 Practical Salinity Scale (PSS-78). All temperature analysis here uses the 1968 International Practical Temperature Scale (IPTS-68), which is applicable to the 1980 equation of state (EOS-80). Accuracies for WOCE stations are believed to be at least 0.003 PSS-78 for salinity, 0.002°C for temperature, and 3 db for pressure, with temperature accuracy approaching 0.001°C for some GO-SHIP cruises.

We screen data prior to analysis based on two criteria. First, only data with good quality flags are used. Second, each section is visually inspected to determine if the trackline of any given occupation was close enough to those of other occupations for comparison. Here the trackline refers to the zonal or meridional line along which the sampling stations fell (as opposed to the locations of the stations themselves), typically following a nominal latitude or longitude (Figs. 1–2). Tracklines of reoccupations of most sections used here lie within 10 km of the original, with four exceptions: First, the four occupations of A05 diverge at the east and west ends of the trackline: on the west end, between 69°W and 76°W, the 1998 and 2004 occupations lie 220 km to the north of the 1981 and 1992 occupations; on the east end, east of 24°W, the 1992 occupation turns northeast and reaches distances of as much as 220 km from the trackline of the three other occupations. Second, the tracklines of the 1993 and 2003 occupations of A16 diverge by up to 88 km between 2°N and 12°N. Third, south of 20°S along P16 the tracklines are consistently about 40 km apart. Finally, between 85°W and 91°W along

I05, the trackline of the 1995 occupation reaches distances as much as 55 km from the tracklines of the 2002 and 2009 occupations. These variations are deemed useable because they fell in areas of small horizontal density gradients. However, in other areas where tracklines diverge by less than 200 km the data are not used here because they were occupied in areas of large horizontal density gradients such as in the Southern Ocean. In addition, any data from tracklines falling on opposite sides of deep ridges are not used in this study.

The sections analyzed here were not necessarily occupied in a single leg by one ship. Many of them were broken into multiple segments that span more than a single calendar year. These segments are aggregated into a single section for this analysis. Sections with more than one occupation in a single calendar year are treated as if all stations measured that year were from one occupation. This aggregation applies to 12 sections: the 1990, 1991, 1992, 1994, 1995, 1996, and 1997 occupations of A01, the 1988/9 occupation of A16, the 1994/5 and 2007 occupations of I08, the 1995 occupation of I09, the 1999 and 2007 occupations of P01, the 1993/4 occupation of P02, the 2005/6 occupation of P03, the 1992 and 2003 occupations of P06, the 1992 and 2005 occupations of P16, the 1991/2/3 occupation of P17, the 1994 and 2008 occupations of P18, and the 1995 occupation of S03.

3. Temperature change analysis

We interpolate data for each occupation of the 26 studied sections onto a closely spaced vertical and horizontal grid along their tracklines for analysis. First, potential temperature (θ) is derived from the 2-dbar CTD data at each station. The station θ

profiles are then low-passed vertically with a 40-dbar half-width Hanning filter and interpolated onto a 20-dbar vertical grid. At each pressure, the data are then interpolated onto an evenly spaced standard 2' longitudinal or latitudinal grid along the section trackline using a space-preserving piecewise cubic Hermite interpolant. The horizontal grid chosen matches a 2' bathymetric dataset derived from merging satellite altimetry data and bathymetric soundings (Smith and Sandwell 1997). The bathymetric dataset and the measured CTD maximum pressures for each station are used to mask interpolated data located below the sea floor. In addition, interpolated data are discarded between any gaps in station spacing exceeding 2° of latitude or longitude along a trackline.

We calculate a rate of change in θ with time ($d\theta/dt$) at every vertical and horizontal grid point along each trackline using data from all occupations of that section where the time between the first and last occupation exceeds 2.5 years. In places with only two occupations, $d\theta/dt$ is calculated by dividing the θ change between occupations by the time between occupations. For sections with more than two occupations, at each grid point, a line is fit to θ data versus time using least squares, allowing estimates of both $d\theta/dt$ and its uncertainty from the slope of the line and its error (Fig. 4). Here we assume that errors owing to spatial and temporal variability discussed immediately below dominate, and so ignore the slope uncertainties and the comparatively small instrumental errors of 0.001–0.002°C. We construct pressure-latitude or pressure-longitude sections of $d\theta/dt$ estimates for each repeat section (e.g., Fig. 5).

Along each trackline, the $d\theta/dt$ section contours reveal vertically banded structures extending throughout the water column (Fig. 5). These vertical structures are most likely due to mesoscale ocean eddies, internal waves, and tides that cause vertical displacements

in isopycnals. To evaluate the statistical significance of the observed changes in θ in the face of such variations, a robust estimate of a typical horizontal decorrelation length scale is required to calculate the effective degrees of freedom (DOF). To evaluate the length scale of these features, at every pressure level along each section, we remove unsampled (masked) grid points, and then find the maximum of the integral of the spatially lagged autocovariance of the spatially detrended warming rate, following Johnson et al. (2008a). Twice this integral gives an estimate of the horizontal decorrelation length scale.

The horizontal decorrelation length scale varies among sections, with values ranging from 25–400 km, but generally clustering near 160 km (Fig. 6). The decorrelation length scales estimated for each section are relatively constant vertically from about 500–5000 dbar because energetic vertical features in $d\theta/dt$ tend to be consistent throughout the water column. Deeper than 5000 dbar, the length scale gradually tends toward zero with depth, as the sampled region gets smaller and smaller, and there are more breaks in the sections owing to intervening topography. Shallower than 500 dbar, the length scales sometimes get longer, perhaps owing to large-scale wind-driven shifts in gyre positions or aliasing of the seasonal cycle. At each pressure surface, using repeat sections with lengths greater than 2000 km, we calculate the median and lower and upper interquartile range of the horizontal decorrelation length scale (Fig. 5). There are 23 sections with lengths greater than 2000 km at that surface but this number decreases with depth to only 12 sections by 5000 dbar. Between 500 and 5000 dbar, the median is fairly constant around 163 km. The vertical mean and median between 500 and 5000 dbar are both 163 km. This value is used throughout this study as our best estimate of the horizontal length scale for all sections at all pressures. We chose the

2000-km section-length criterion based on an examination of decorrelation-length scale estimates vs. section length (not shown). For sections longer than 2000-km the decorrelation-length scale estimates appear to asymptote toward common values. This requirement ensures the sections used for the decorrelation length-scale estimate sample this length scale roughly a dozen times or more.

For this analysis we divide the ocean into 32 deep basins (Fig. 1) based on bottom topography (Smith and Sandwell 1997) and climatological ocean bottom temperature (Gouretski and Koltermann 2004). The boundaries for the basins follow the major ocean ridges, most of which are shallower than 3000 m. Most of the 32 deep basins were crossed by at least one section, with the exception of the Arabian Sea and Somali Basin in the northwest Indian Ocean (Fig. 1). A few marginal seas (the Sea of Okhotsk, Sea of Japan, Philippine Sea, Guatemala Basin, Panama Basin, and Gulf of Mexico) are unsampled, but these are all mostly shallower than 4000 dbar, and thus have a minor impact on our study. The Arctic Ocean and Nordic Seas, which contain little or no AABW, were not sampled by repeat sections analyzed here, and thus are not included in this study.

We estimate a mean warming rate and its associated uncertainty at each pressure horizon for each of the 32 deep basins sampled (e.g., Fig. 7). For these estimates, the sections are divided at the basin boundaries and the mean and standard deviations of the warming rates on isobars within each basin are calculated. If a basin only has one section crossing it, the means and standard deviations for the single section within the basin as a function of pressure are assumed to be representative of the whole basin. If a basin is crossed by more than one section, the length-weighted means and standard deviations are

calculated using data from portions of all sections crossing the basin at each pressure level. For example, the mean $d\theta/dt$ for the Southeast Pacific Basin (Fig. 7) estimates warming of about 0.002°C yr^{-1}, statistically different from zero at 95% confidence below about 3500 m. This result might be anticipated from examination of the warming rate along the P18 section (Fig. 5), which is the major contributor to this estimate, augmented only by a small portion of the southern end of P16 that also enters the basin (Fig. 1).

At each pressure level, we compute the DOF for each section crossing the basin by dividing the horizontal length of the section at the given pressure by a single horizontal decorrelation length scale of 163 km. In areas where topography isolates the sampled regions such that one region is continuously sampled in the horizontal over a distance less than the decorrelation length scale, and that region is separated from adjacent sampled regions by distances more than the decorrelation length scale, the data from the region in question are assumed to be statistically independent and to contribute one DOF to the estimate. The DOF at each pressure within each basin is the sum of the DOF for all sections that cross that basin. The standard deviation is converted to a standard error by dividing by the square root of the DOF and the 95% confidence interval is estimated by applying Student's t-test.

In basins where the sampled data do not extend to the bottom, the deepest estimate of $d\theta/dt$ is extended to the bottom of the basin. Each basin is visually inspected to make sure that the bottom measurement is well below the sill depth of that basin and that the volume of water below the bottom measurement is small compared to the volume of the basin.

In addition to these basin-based warming estimates using physical topographical boundaries, we make one other estimate of $d\theta/dt$ for the entire Southern Ocean. We use an estimate of the location of the SubAntarctic Front (SAF; Orsi et al., 1995), which demarks the northern edge of the ACC, as the northern boundary for the region. Even though it is not a physical boundary, the SAF acts as a dynamical boundary separating water masses. South of the SAF, isotherms rise steeply, indicating that the cold dense water of Antarctic origins found only in very deep regions to the north of the SAF extends to shallower ranges of the water column to the south of the SAF (Fig. 5). The eight meridional and one zonal section that sample regions south of the SAF (Fig. 2) are grouped together to estimate the warming rate along pressure horizons in the Southern Ocean. The meridional sections are reasonably evenly spaced around the globe and give good coverage of the South Indian and South Atlantic Oceans. However, there is only one section in the South Pacific Ocean (P18, located on the eastern side) that extends to the continental shelf, so this region is under-represented in the final estimates of Southern Ocean changes.

The warming rate of the entire Southern Ocean is estimated at each pressure. Using the same method described above for basins with multiple crossings, the nine sections with data south of the SAF (Fig. 2) are used to find the length-weighted means and 95% confidence intervals of the warming rate in the Southern Ocean. As mentioned earlier, due to the spatial distribution of available data, these values are slightly biased toward θ changes in the South Indian and South Atlantic Oceans over the South Pacific Ocean and thus might be more representative of property changes originating from Weddell Sea or Adelie Land Bottom Water rather than those originating from Ross Sea Bottom Water.

In addition, since not all the tracklines extend to the continental shelf (Fig. 2), the northern portions of the Southern Ocean may be over represented in the warming rates for the Southern Ocean presented here.

4. Heat gain and sea level rise

We focus here on the effects of 1990s to 2000s warming of cold waters of Antarctic origin, which we loosely term AABW, on local and global heat and sea level budgets. To this end we estimate heat gains and the contribution to SLR from warming in basins, and globally, for depths greater than 4000 m. In many of the basins north of the SAF, warming trends on pressure levels become significantly different from zero at 95% confidence below around 4000 m, where the AABW signature is strongest, making this pressure level a natural division for this study. In the Southern Ocean, south of the SAF, the AABW influence extends much higher in the water column (Johnson 2008), as does consistently strong warming, so we also analyze contributions to sea level rise and heat gain from warming found from 1000–4000 m in the Southern Ocean (south of the SAF). We sum the changes found in these two regions (1000–4000 m south of the SAF and below 4000 m everywhere but the Arctic Ocean and Nordic Seas) to estimate the effects of warming of AABW on global heat and SLR budgets.

a. Local estimates

To calculate the contribution of warming in each basin below 4000 m to the heat budget, $d\theta/dt$ estimates are converted to a heat flux (Q_i) through the 4000 m isobath of each basin using:

$$Q_i = \frac{\int_{4000}^{bottom} \rho \cdot C_p \cdot d\theta/dt \cdot a_i(z) \cdot dz}{a_i(4000)}, \quad (1)$$

where *a(z)* is the surface area of each depth, *z*, calculated using the satellite bathymetric dataset (Smith and Sandwell 1997). Profiles of density, ρ, and heat capacity, C_p, are estimated in each basin using the climatological mean temperature and salinity at each pressure for the basin in question. The integral in (1) gives the total heating rate below 4000 m. Dividing by the surface area at 4000 m, $a_i(4000)$, converts the total heating rate into a flux required through the 4000 m level to account for the observed warming beneath that level (Fig. 8).

We find the 95% confidence interval associated with the *Q* for each basin using the volume-weighted variance of *Q* and volume-weighted DOF for that basin. The variance (standard deviation squared) of $d\theta/dt$ at each pressure in the basin is converted to a heating rate variance by multiplying by the square of $\rho \cdot C_p$. Then the volume-weighted means for the variance and DOF below 4000 m is found using *a(z)* for weights in a vertical integration. The standard deviation is then found by the taking the square root of the variance; and the 95% confidence interval estimated using the Student's t-test (Fig. 8).

Similarly, we calculate the local sea level rise due to thermal expansion of each basin below 4000 m using:

$$F_i = \frac{\int_{4000}^{bottom} \alpha \cdot d\theta/dt \cdot a(z) \cdot dz}{a_i(4000)}, \quad (2)$$

where α is the thermal expansion coefficient. The associated 95% confidence intervals for each F_i are estimated following a method analogous to that described above for the global heat budget contribution (Fig. 9).

The geographical distributions of basin-mean warming and cooling below 4000 m from the 1990s to the 2000s (Fig. 8) and associated SLR changes (Fig. 9) reveal a clear global pattern. Of the 24 basins with data below 4000 m, 15 warmed (nine significantly different from zero at 95% confidence) and 9 cooled (one significantly different from zero at 95% confidence).

In general, a clear pattern in the magnitude of abyssal heating is seen: smaller values further to the north and larger values to the south (Figs. 8–9). The three southernmost basins: the Weddell-Enderby Basin, the Australian-Antarctic Basin, and the Southeast Pacific Basin show strong warming below 4000 dbar of 0.33 (±0.28), 0.24 (±0.14), and 0.15 (±0.11) W m^{-2} respectively, all significantly different from zero at 95% confidence. We can trace the propagation of AABW from these southernmost basins northward, and with it, a waning warming (or cooling) signal. In each of the three oceans, AABW flows generally north from basin to basin, subject to bathymetric constraints. However, the Atlantic, Indian, and Pacific Oceans each present a slightly different pattern that should be viewed with the AABW flow in mind, as discussed below.

In the Atlantic Ocean, the warming pattern follows the flow of AABW out of the Southern Ocean. AABW leaves the Weddell Sea through the Sandwich Trench traveling toward the western North Atlantic through the Argentine and Brazil Basins in the western South Atlantic (Coles et al. 1996; Orsi et al. 1999). The Argentine and Brazil Basins,

containing mostly AABW in the abyss (Johnson 2008), show statistically significant warming, while the western North Atlantic, which contains little AABW influence, shows only a small amount of warming, not significantly different from zero (Fig. 8). At the equator, some AABW flow crosses into the Angola Basin and travels north and south filling the basins east of the Mid-Atlantic Ridge (Warren and Speer, 1991). These eastern Atlantic basins all show cooling with the northernmost basin being the only statistically significantly cooling basin found in this study. However, the dominant abyssal influence in these eastern basins is NADW, not AABW (Johnson 2008). On the other hand, the strong and statistically significant recent warming in the deep Caribbean Sea (Figs. 8–9), filled with NADW, is part of a trend starting a few decades prior to the 1990s (Johnson and Purkey 2009).

In the Indian Ocean both warming and cooling basins are found (Figs. 8–9). Basins to the west of the Ninetyeast Ridge mostly show deep cooling, although none of these basins exhibit cooling significantly different from zero at 95% confidence, while the two basins to the east of the ridge show statistically significant warming. Two of the basins west of the Ninetyeast Ridge, the Somali Basin and Arabian Sea, are not sampled. Since the deepest sills of these basins connect them to adjacent basins exhibiting cooling, one could speculate that these unsampled basins might have shown cooling had they been sampled repeatedly, although the adjacent cooling is not statistically different from zero at 95% confidence. As in the Atlantic, the magnitude of the warming (or cooling) in the Indian Ocean basins decreases with distance from the Southern Ocean. The warming Agulhas-Mozambique Basin, located directly south of Africa between the cooling Cape Basin in the southeast Atlantic Ocean and the cooling Crozet and Madagascar Basins in

the southwest Indian Ocean, stands out as an anomaly to this pattern. Data from two tracklines crossing the dynamic Agulhas-Mozambique Basin were used in this calculation (Fig. 1): I05 shows uniform cooling across the northeast region of the basin; but I06 alternates between warming and cooling while crossing the fronts of the ACC. Hence these data estimate overall warming in the basin, but with a large uncertainty.

In contrast to the Atlantic and Indian Oceans, the Pacific Ocean (Figs. 8–9) exhibits deep warming that is significantly different from zero at 95% confidence in all its main central basins with more uncertain warming in most of the small peripheral basins. Two of the peripheral basins showed very slight (0.03 and 0.01 W m^{-2}) but statistically insignificant cooling. Similarly to the other two oceans, the magnitude of the warming in the Pacific basins decreases northward from the Southern Ocean.

To complement the local estimates of warming and SLR below 4000 m, Q and F are calculated for the region between 1000–4000 m in the Southern Ocean, where AABW influence is also strong (Johnson 2008). Equations (1) and (2) are applied following the same procedure as described above but using the area and $d\theta/dt$ from the Southern Ocean. The heating between 1000 and 4000 m in the region contributes an additional heat flux of 0.86 (±0.84) W m^{-2} and 0.87 (±0.83) mm yr^{-1} to the local heat flux and SLR, respectively. Adding these changes to the heat flux and SLR below 4000 m in the Southern Ocean yields local heat gains equivalent to a local heat flux on the order of 1 W m^{-2} and SLR on the order of 1 mm yr^{-1}.

b. Global estimates

The observed regional heat flux and SLR are combined in a rough estimate of the recent AABW warming's contribution to global heat and SLR budgets. The total heat flux and error at each depth can be calculated by summing the results from all basins using

$$Q_{abyssal} = \frac{\sum_{b=1}^{32} \rho \cdot C_p \cdot d\theta/dt_b(z) \cdot a_b(z) \cdot dz}{SA_{earth}} \tag{3}$$

and the 95% confidence interval on that sum estimated using

$$err_{95\%} = \frac{\sqrt{\sum_{b=1}^{32} (\rho \cdot C_p \cdot \sigma_{d\theta/dt\,b} \cdot a_b)^2}}{SA_{earth}} \times 2, \tag{4}$$

where SA_{earth} is the total surface area of the earth and b denotes each basin (Fig. 10a). The factor of 2 in (4) is a conservative estimate of Student's t-test value for 95% confidence. The DOF of the 24 basins range from 2–239 with a mean and median of 29 and 15. Each basin is independent, making the DOF easily over 60, thus this factor could arguably be less than 2.

The contribution of the Southern Ocean Q (Fig. 10b) to the global heat budget can be derived by dividing by SA_{earth} instead of the basin surface area in (1). Comparing the total global heat flux (Fig. 10a) to the heat flux south of the SAF (Fig. 10b) further emphasizes the result (Figs. 8–9) that the Southern Ocean warming accounts for a substantial fraction of the observed global changes in deep (but not abyssal) temperature. Above 4000 m almost all the deep warming can be accounted for by warming in the Southern Ocean, supporting the choice made here of focusing on global abyssal changes below 4000 m, and Southern Ocean deep changes from 1000–4000 m.

We make an estimate of the total heat gain from recent AABW warming by adding the integral of $Q_{abyssal}$ below 4000 m to the integral of $Q_{SouthernOcean}$ from 1000 m to 4000 m (Table 1). The 95% confidence interval for $Q_{abyssal}$ is calculated as the square root of the sum of the basin standard errors squared times 2, again using this factor because the DOF exceed 60. The warming below 4000 m is found to contribute 0.024 (±0.010) W m^{-2}. The Southern Ocean between 1000–4000 m contributes an additional 0.065 (±0.063) W m^{-2}, for a total of 0.089 (±0.064) W m^{-1} (Table 1). Following the same procedure, AABW's contribution to SLR due to thermal expansion can be estimated using α instead of $\rho \cdot C_p$ and the surface area of the ocean instead of the surface area of the globe. A total of 0.0134 (±0.086) mm yr^{-1} of SLR can be linked to the thermal expansion of AABW (Table 1).

The above calculations assume that the unsampled basins have zero contribution to the heat budget. We investigate the effects of two alternative scenarios on the estimates. For the first scenario, we assume that the unsampled basins have a $d\theta/dt$ value equal to the mean $d\theta/dt$ of all the sampled basins. This scenario increases our global abyssal estimate by 0.0005 W m^{-2}. For the second scenario, we assume that the unsampled basins have a $d\theta/dt$ equal to the $d\theta/dt$ of the adjacent basin with the deepest connecting sill upstream in terms of AABW flow, where the abyssal water supplying the basin in question likely originated. The two unsampled deep basins in the Indian Ocean: the Somali Basin and Arabian Sea, are assumed to be connected to the Madagascar Basin and Mid-Indian Basin, respectively. In addition, $d\theta/dt$ of the Pacific Basin is used for the Sea of Okhotsk, Sea of Japan, and the Coral Sea and $d\theta/dt$ of the Peru Basin is used for the Guatemala and Panama Basins. However, as mentioned earlier, all of these basins are

either completely or mostly shallower then 4000 m: therefore, they have little impact on the estimates given here. The scenario decreases the global mean estimate of AABW heat gain by 0.0009 W m^{-2}. Thus, for either of these methods of accounting for the unsampled basins, the global values remain identical at the quoted precision (Table 1).

In addition to using 4000 m as the shallower limit for the abyssal estimate and the deeper limit for the Southern Ocean estimate of AABW warming, we also present global heat flux and SLR estimates using 3000 m for that dividing depth (Table 1). We believe that 4000 m is the more appropriate choice for quantifying the effects of AABW warming. However, since the deepest known studies of ocean heat uptake of which we are aware extend only to 3000 m (Levitus et al. 2005), we calculate the flux and SLR below 3000 m for comparison with this previous work. When 3000 m is used instead of 4000 m, the same basin patterns emerge (not shown). The only basin where the mean changes sign is the Peru Basin, which goes from cooling at 0.01 W m^{-2} to warming at 0.03 W m^{-2}. The error to signal ratio for abyssal heating rates below 3000 m increases substantially in many of the basins compared with that below 4000 m, with only seven of the basins' warming below 3000 m being significantly different from zero at 95% confidence and none of the basins' cooling being statistically significant.

Again, following (3) and (4), the global heat flux to the deep ocean can be estimated by adding $Q_{abyssal}$ below 3000 m to the $Q_{SouthernOcean}$ between 1000 and 3000 m (Table 1). As expected, using this 3000-m interface the deep contribution below 3000 m around the globe increases compared to that below 4000 m. The Southern Ocean contribution between 1000 and 3000 m is also less than between 1000 and 4000 m. The sum, however, is roughly the same. Again, this similarity exists because most of the observed

warming between 3000 and 4000 m is located in the Southern Ocean, and therefore, choosing 4000 or 3000 m north of the SAF does not change the heat gained by the abyssal ocean there. However, the partition of error associated with the estimates shifts as the interface depth is changed. The abyssal contribution has a signal 2.5 times its 95% confidence with the 4000-m interface, but only 1.5 times its confidence using 3000 m, because the bottom-intensified abyssal warming signal is most robust near the bottom.

5. Discussion

We make three large assumptions in constructing the abyssal basin estimates of heat gain and sea level rise below 4000 m and the deep Southern Ocean estimates of these quantities from 1000–4000 m. First, we assume that $d\theta/dt$ within a given basin or the Southern Ocean is relatively consistent over the pressure intervals considered. This assumption is often supported by examination of pressure-latitude/longitude sections of $d\theta/dt$ estimates, wherein $d\theta/dt$ often appears to be roughly vertically uniform on deep pressure horizons, and more so below the sill depth of a basin. For example, P18 crosses four basins: the Southeast Pacific Basin, Chile Basin, Peru Basin, and Pacific Basin (Fig. 5). The Chile and Peru basins both show uniform (but small) warming below 3000 m and exhibit little variability, while the Southeast Pacific Basin shows stronger warming but also higher variability. Second, we assume that the tracklines used to estimate warming rates in each basin or region are representative samples of that basin. The validity of this assumption is dependent on the spatial coverage of the tracklines. In the basins that have multiple meridional and zonal crossings, this assumption seems valid. However, in a few of the basins, such as in the Philippine Sea and the Southeast Pacific

Basin, repeat sections cross only a small portion of the basin. In these cases, the changes seen in the single region are applied to the whole basin (Fig. 1). Generally, the error analysis ensures that the uncertainties for these basins, with their limited DOF, are appropriately large. The third assumption is that the timescale of the $d\theta/dt$ changes observed is longer than the intervals between occupations. This assumption generally seems valid because different sections taken over different time intervals in the same basin yield similar estimates of $d\theta/dt$, and, as has been shown above, a consistent large-scale geographical pattern emerges from the analysis.

While we focus on deep warming of Antarctic origin here, the temperature and salinity of NADW also varies significantly on interdecadal time scales (Yashayaev and Clarke 2008), with implications for long-term warming (Levitus et al. 2005). Our study includes some of this recent variability, especially in the abyssal North Atlantic. However, the deep Nordic Seas have also warmed at a rate around 0.01°C yr^{-1} during the 1990s (Osterhus and Gammelsrod 1999; Karstensen et al. 2005). The local heat flux that would be needed to account for the warming in the Greenland sea below 1500 m since 1989 is on the order of 50 W m^{-2} (Karstensen et al. 2005), with a similar value for the warming in the deep Norwegian Sea starting in 1980 (Osterhus and Gammelsrod 1999). These marginal seas are not ventilated by AABW, and are excluded from our study. However, if the Arctic Ocean and Nordic Seas had been included, the global heat flux estimates for below 3000 m and 4000 m presented here could have increased.

The heating reported here is a substantial fraction of previously reported upper ocean heat uptake. The upper 3000 m of the global ocean has been estimated to warm at a rate equivalent to a heat flux of 0.20 W m^{-2} over the entire surface of the Earth between

1955 and 1998 with most of the warming contained in the upper 700 m of the water column (Levitus et al. 2005). From 1993 to 2003 the warming of the upper 700 m of the global ocean has been reported as equivalent to a heat flux of 0.5 ± 0.18 W m^{-2} over the globe (Bindoff et al. 2007). Here, we showed the heat uptake by AABW contributes about 0.09 W m^{-2} to the global heat budget. Thus, including the deep ocean in the global ocean heat uptake budget could increase the estimated ocean heat uptake over the last decade or so by roughly 20%. While this warming only contributes to a small fraction of the global SLR budget, the local contribution from deep warming in some regions, such as the Southern Ocean (Fig. 9), is on the same order of magnitude as the upper ocean's contribution. Thus, the warming of the deep ocean is contributing a substantial fraction of the heat and sea level rise budgets and needs to be considered to assess the role of the ocean in climate accurately.

The warming reported here is likely due to two different processes, depending on the location. The abyssal warming in the Southern Ocean could be partly caused by advection of warmer water directly from the source. These basins are located directly downstream from the source regions for AABW and are filled on timescales captured by the data used in this study, as shown by transient tracer burdens (Orsi et al. 1999). Outside of the Southern Ocean, where the bottom water advection time back to the source can reach order 1000 years in some regions, the changes can still be tied back to upstream variations communicated on decadal timescales through Kelvin and Rossby Waves (Nakano and Suginohara 2002). Property or formation rate changes at the sources of AABW could slow the southern branch of the MOC, with these planetary waves effecting

remote retractions of deep water in the vertical and horizontal, explaining the abyssal warming reported here, some far from the Southern Ocean.

To gain more precise estimates of the deep ocean's contribution to sea level and global energy budgets, and to understand better how the warming signal of AABW spreads from the Southern Ocean around the globe, higher spatial and temporal resolution sampling of the deep ocean is required. The basin space-scale and decadal time-scale resolution of the data used here could be aliased by smaller spatial scales and shorter temporal scales. Furthermore, the propagation of the signal can only be conjectured, not confirmed, with the present observing system.

In summary, we show that the abyssal ocean has warmed significantly since the 1980s (Table 1). The deep warming did not occur uniformly around the globe but is amplified to the south and fades to the north (Fig. 8). Both the Indian and Atlantic Oceans only warmed on one side, with statistically insignificant cooling on their other side. The recent decadal warming of the abyssal global ocean below 4000 m is equivalent to a global surface energy imbalance of 0.024 (±0.010) W m^{-2} with Southern Ocean deep warming contributing an additional 0.065 (±0.063) W m^{-2} between 1000 and 4000 m. The warming contributes about 0.1 mm yr^{-1} to the global sea level rise. However, in the Southern Ocean, the warming below 1000 m contributes about 1 mm yr^{-1} locally. Thus, deep ocean warming contributions need to be considered in sea level rise and global energy budgets.

Acknowledgments. Our heartfelt thanks go to all those who helped to collect, calibrate, and process the WOCE and GO-SHIP data analyzed here. Discussions with

John Lyman were useful. The findings and conclusions in this article are those of the authors and do not necessarily reflect the views of the National Oceanic and Atmospheric Administration (NOAA). The NOAA Climate Program Office and the NOAA Office of Oceanic and Atmospheric Research supported this research.

REFERENCES

Aoki, S., S. R. Rintoul, S. Ushio, S. Watanabe, and N. L. Bindoff, 2005: Freshening of the Adélie Land Bottom Water near 140°E. *Geophys. Res. Lett.,* **32**, L23601, doi:10.1029/2005GL024246.

Bindoff, N. L., J. Willebrand, V. Artale, A, Cazenave, J. Gregory, S. Gulev, K. Hanawa, C. Le Quéré, S. Levitus, Y. Nojiri, C. K. Shum, L. D. Talley, and A. Unnikrishnan, 2007: Observations: Oceanic Climate Change and Sea Level. In: *Climate Change 2007: The Physical Science Basis. Contribution of Working Group I to the Fourth Assessment Report of the Intergovernmental Panel on Climate Change* [Solomon, S., D. Qin, M. Manning, Z. Chen, M. Marquis, K.B. Averyt, M. Tignor and H.L. Miller (eds.)]. Cambridge University Press, Cambridge, United Kingdom and New York, NY, USA.

Böning, C. W., A. Dispert, M. Visbeck, S. R. Rintoul, and F. U. Schwarzkopf, 2008: The response of the Antarctic Circumpolar Current to recent climate change. *Nature Geosci.*, **1**, 864–869.

Boe, J., A. Hall, and X. Qu, 2009: Deep ocean heat uptake as a major source of spread in transient climate change simulations. *Geophys. Res. Lett.*, **36**, L22701, doi: 10.1029/2009GL040845.

Cazenave, A., A. Lombard, and W. Llovel, 2008: Present-day sea level rise: A synthesis. *Comptes rendus Geosci.,* **340** , 761–770.

Coles, V. J., M. S. McCartney, D. B. Olson, and W. M. Smethie Jr., 1996: Changes in Antarctic Bottom Water properties in the western South Atlantic in the late 1980s. *J. Geophys. Res*., **101**, 8957–8970.

Domingues, C. M., J. A. Church, N. J. White, P. J. Gleckler, S. E. Wijffels, P. M. Barker, and J. R. Dunn, 2008: Improved estimates of upper-ocean warming and multi-decadal sea-level rise. *Nature*, **453**, 1090–1093, doi:10.1038/nature07080.

Fahrbach, E., M. Hoppema, G. Rohardt, M. Schroder, A. Wisotzki, 2004: Decadal-scale variations of water mass properties in the deep Weddell Sea. *Ocean Dynamics*, **54**, 77–91.

Fukasawa, M., H. Freeland, R. Perkin, T. Watanabe, H. Uchida, and A. Nishima, 2004: Bottom water warming in the North Pacific Ocean. *Nature*, **427**, 825–827.

Gille, S. T., 2002: Warming of the Southern Ocean since the 1950s. *Science*, **295**, 1275–1277.

Gille, S. T., 2008: Decadal-scale temperature trends in the Southern Hemisphere ocean. *J. Climate*, **21**, 4749–4765.

Gouretski, V. V., and K. P. Koltermann, 2004: *WOCE Global Hydrographic Climatology*. Berichte des Bundesamtes für Seeschifffahrt und Hydrographie, *35*, pp. 52 + 2 CD-ROMs.

Hansen, J., L. Nazarenko, R. Ruedy, M. Sato, J. Willis, A. Del Genio, D. Koch, A. Lacis, K. Lo, S. Menon, T. Novakov, J. Perlwitz, G. Russell, G. A. Schmidt, and N. Tausnev, 2005: Earth's energy imbalance: Confirmation and implications. *Science*, **308**, 1431–1435.

Jacobs, S. S., C. F. Giulivi, and P. A. Mele, 2002: Freshening of the Ross Sea during the late 20th century. *Science*, **297**, 386–389.

Johnson, G. C., 2008: Quantifying Antarctic Bottom Water and North Atlantic Deep Water volumes. *J. Geophys. Res*., **113**, C05027, doi: 10.1029/2007JC004477.

Johnson, G. C., and S. C. Doney, 2006: Recent western South Atlantic bottom water warming. *Geophys. Res. Lett*., **33**, L14614, doi:10.1029/2006GL026769.

Johnson, G. C., S. Mecking, B. M. Sloyan, and S. E. Wijffels, 2007: Recent bottom water warming in the Pacific Ocean. *J. Climate*, **20**, 5365–5375.

Johnson, G. C., and S. G. Purkey, 2009: Deep Caribbean Sea warming. *Deep-Sea Res. I*, **56**, 827–834, doi:10.1016/j.dsr.2008.12.011.

Johnson, G. C., S. G. Purkey, and J. L. Bullister, 2008a: Warming and freshening in the abyssal southeastern Indian Ocean. *J. Climate*, **21**, 5353–5365.

Johnson, G. C., S. G. Purkey, and J. M. Toole, 2008b: Reduced Antarctic meridional overturning circulation reaches the North Atlantic Ocean. *Geophys. Res. Letters,* **35**, L22601, doi: 10.1029/2008GL03519.

Karstensen, J., P. Schlosser, D. W. R. Wallace, J. L. Bullister and J. Blindheim, 2005: Water mass transformation in the Greenland Sea during the 1990s. *J. Geophys. Res.*, **110**, C07022, doi: 10.1029/2004JC002510.

Kawano, T., M. Fukawasa, S. Kouketsu, H. Uchida, T. Doi, I. Kaneko, M. Aoyama, and W. Scheider, 2006: Bottom water warming along the pathways of lower circumpolar deep water in the Pacific Ocean. *Geophys. Res. Lett*., **33**, L23613, doi:10.1029/2006GL027933.

Kouketsu, S., M. Fukasawa, I. Kaneko, T. Kawano, H. Uchida, T. Doi, M. Aoyama, and K. Murakami, 2009: Changes in water properties and transports along 24°N in the North Pacific between 1985 and 2005. *J. Geophys. Res.*, **114**, C01008, doi:10.1029/2008JC004778.

LeBel, D. A., W. M. Smethie Jr., M. Rhein, D. Kieke, R. A. Fine, J. L. Bullister, D.-H. Min, W. Roether, R. F. Weiss, C. Andrié, D. Smythe-Wright, E. P. Jones, 2008: The formation rate of North Atlantic Deep Water and Eighteen Degree Water calculated from CFC-11 inventories observed during WOCE. *Deep-Sea Res. I,* **55**, 891–910.

Levitus, S., J. Antonov, and T. Boyer, 2005: Warming of the world ocean, 1955–2003. *Geophys. Res. Lett.,* **32**, L02604, doi: 10:1029.2004GL021592.

Lumpkin, R., and K. Speer, 2007: Global Ocean meridional overturning. *J. Phys. Oceanogr*., **37**, doi: 10:1175/JPO3130.1.

Meehl. G. A., W. M. Washington, W. D. Collins, J. M. Arblaster, A. Hu, L. E. Budja, W. G. Strand, and H. Teng, 2005: How much more Global Warming and sea level rise? *Science*, **307**, 1769–1772.

Meredith, M. P., A. C. Naveira Garabato, A. L. Gordon, and G. C. Johnson, 2008: Evolution of the Deep and Bottom Water of the Scotia Sea, Southern Ocean, during 1995–2005. *J. Climate*, **21**, 3327–3343.

Miller, L., and B. C. Douglas, 2004: Mass and volume contributions to twentieth-Century global sea level rise. *Nature*, **248**, 406–409.

Murphy, D. M., S. Solomon, R. W. Portmann, K. H. Rosenlof, P. M. Forster, and T. Wong, 2009: An observationally based energy balance for the Earth since 1950. *J. Geophys. Res.*, **114**, D17107, doi:10.1029/2009JD012105.

Nakano, H., and N. Suginohara, 2002: Importance of the eastern Indian Ocean for the abyssal Pacific. *J. Geophys, Res.*, **107**, 3219, doi:10.1029/2001JC001065.

Orsi, A. H., G. C. Johnson, and J. L. Bullister, 1999: Circulation, mixing, and production of Antarctic Bottom Water. *Prog. Oceanogr.*, **43**, 55–109.

Orsi, A. H., T. Whitworth III, and W. D. Nowlin, Jr., 1995: On the meridional extent and fronts of the Antarctic Circumpolar Current. *Deep-Sea Res. I*, **42**, 641–673.

Osterhus, S., and T. Gammelsrod, 1999: The abyss of the Nordic Seas is warming. *J. Climate*, **12**, 3297–3304.

Ozaki H., H. Obata, M. Naganobu, and T. Gamo, 2009: Long-term bottom water warming in the North Ross Sea. *J. Oceanogr.,* **65**, 235–244.

Raper, S. C. B., and R. J. Brathwaite, 2006: Low sea level rise projections from mountain glaciers and icecaps under global warming. *Nature*, **439**, 311–313.

Raper, S. C. B., J. M. Gregory, and R. J. Stouffer, 2002: The role of climate sensitivity and ocean heat uptake on AOGCM transient temperature response. *J. Climate,* **15**, 124–130.

Rintoul, S. R., 2007: Rapid freshening of Antarctic Bottom Water formed in the Indian and Pacific Oceans. *Geophys. Res. Lett.*, **34**, L06606, doi:10.1029/2006GL028550.

Smith, W. H. F., and D. T. Sandwell, 1997: Global seafloor topography from satellite altimetry and ship depth soundings. *Science*, **277**, 1956–1962.

Solomon, S., D. Qin, M. Manning, Z. Chen, M. Marquis, K. B. Averyt, M. Tignor, and H.L. Miller (eds.), 2007: Climate Change 2007: The Physical Basis. Contribution of Working Group I to the Fourth Assessment Report of the Intergovernmental Panel on Climate Change**,** Cambridge University Press, Cambridge, United Kingdom and New York, NY, USA.

Trenberth, K. E, and J. T. Fasullo, 2009: Changes in the flow of energy through the Earth's climate system. *Meteorologische Zeitschrift*, **18**, 369–377.

Warren, B. A., and K. G. Speer, 1991: Deep circulation in the eastern South Atlantic Ocean. *Deep-Sea Res.*, **38(Suppl.)**, S281–S322.

Willis, J. K., D. P. Chambers, and R. S. Nerem, 2008: Assessing the globally averaged sea level budget on seasonal to interannual timescales. *J. Geophys. Res.,***113**, C06015, doi:10.1029/2007JC004517.

Yashayaev, I., and A. Clarke, 2008: Evolution of North Atlantic water masses inferred from Labrador Sea salinity series. *Oceanogr.*, **21**, 30–45.

Zenk, W., and E. Morozov, 2007: Decadal warming of the coldest Antarctic Bottom Water flow through the Vema Channel. *Geophys. Res. Lett.*, *34*, L14607, doi:10.1029/2007GJ030340.

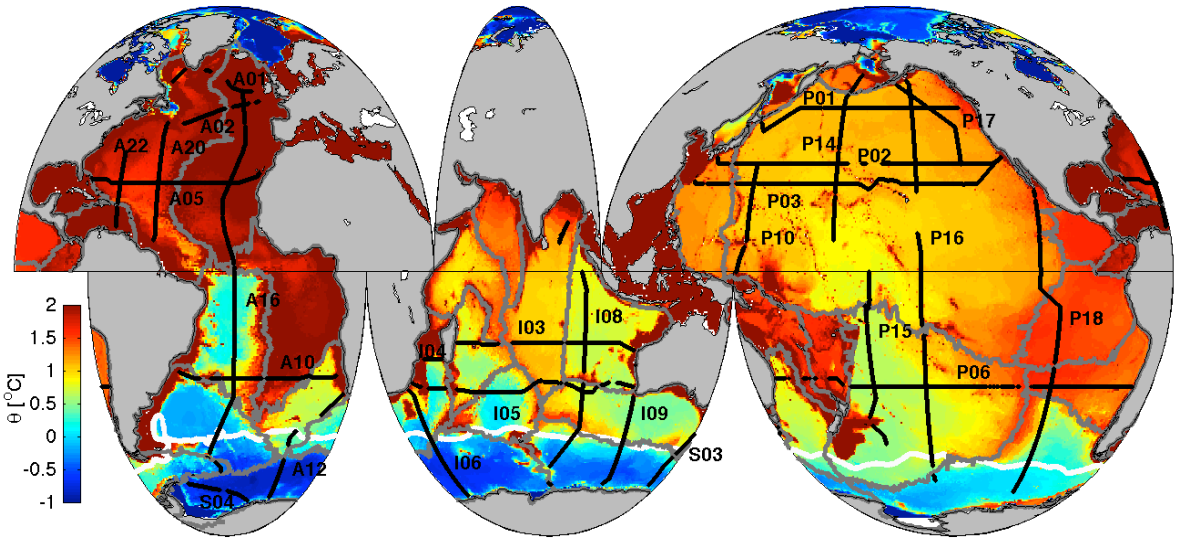

FIG. 1. Tracklines of the 26 repeated sections studied (black lines) with WOCE designators noted adjacent. Basin boundaries are outlined (gray lines) over bottom potential temperature (color) from a WOCE global hydrographic climatology (Gouretski and Koltermann 2004). The Sub Antarctic Front (SAF) position is also shown (white line)

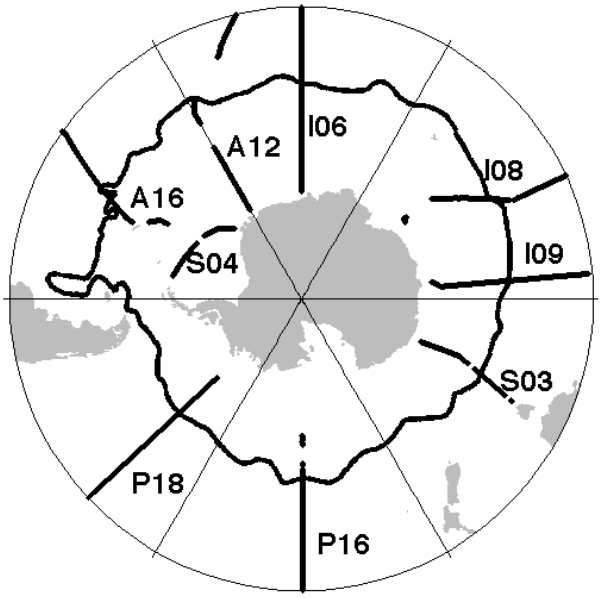

FIG. 2. Polar projection of the nine repeated tracklines (straight lines) that extend into the Southern Ocean south of the SAF (curved line).

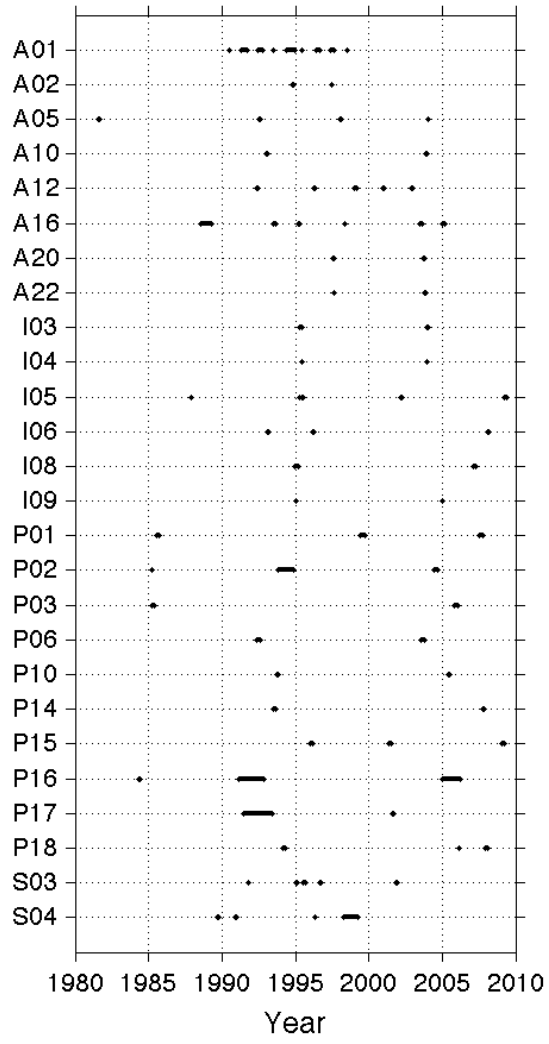

FIG. 3. Occupation dates for each of the 26 repeated sections listed by their WOCE designators (see Fig. 1 for locations). Lines extend over the entire time period over which data were collected for a given occupation of a section. Longer lines indicate where multiple legs of sections taken over the course of up to a year or more are appended for this analysis.

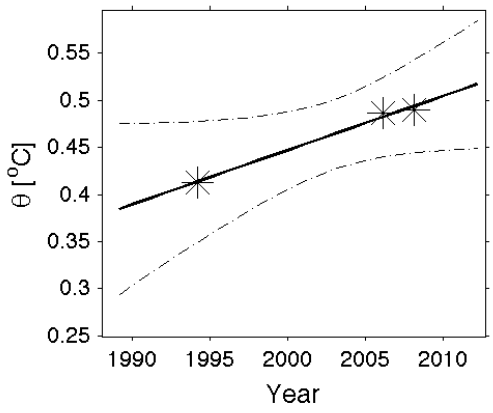

FIG. 4. Local $d\theta/dt$ estimate for a location with more than two section occupations. Potential temperature data (asterisks) from three occupations along P18 (see Fig. 1 for location) at 56°S and 4000 dbar plotted vs. time are used to fit a line by least squares (sold line), producing an error estimate here shown as 95% confidence limits (dotted line). The slope of the line is $d\theta/dt$.

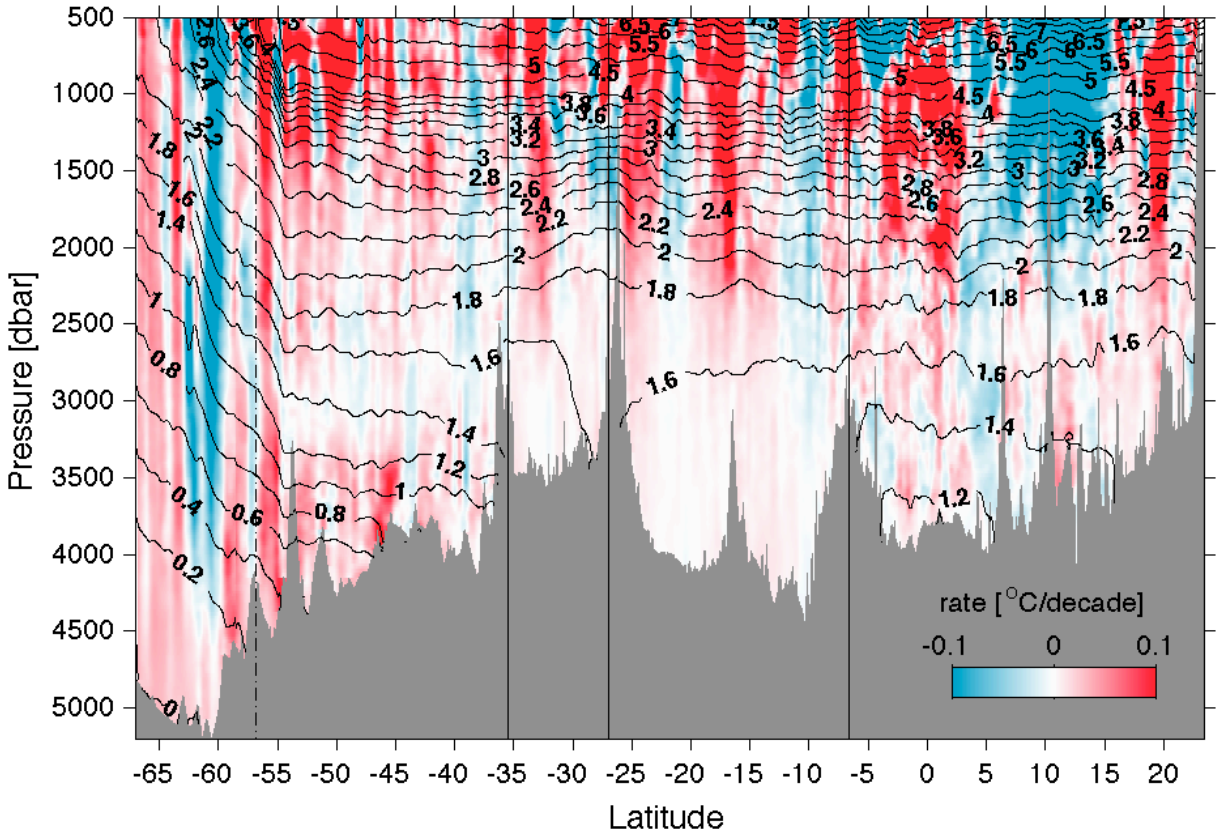

FIG. 5. Time rate of change of θ, $d\theta/dt$ (color, see key), along the trackline of P18 (see Fig. 1 for location). Areas of warming are shaded in red and regions of cooling are shaded in blue with intensity scaled by the magnitude of the warming. Mean θ values over all occupations are contoured (black lines). This trackline is grouped into four basins for analysis (boundaries shown by vertical black lines), and the area south of the SAF (vertical dot-dashed line) is also analyzed separately. The basins from south to north are the Southeast Pacific Basin, Chile Basin, Peru Basin, and Pacific Basin.

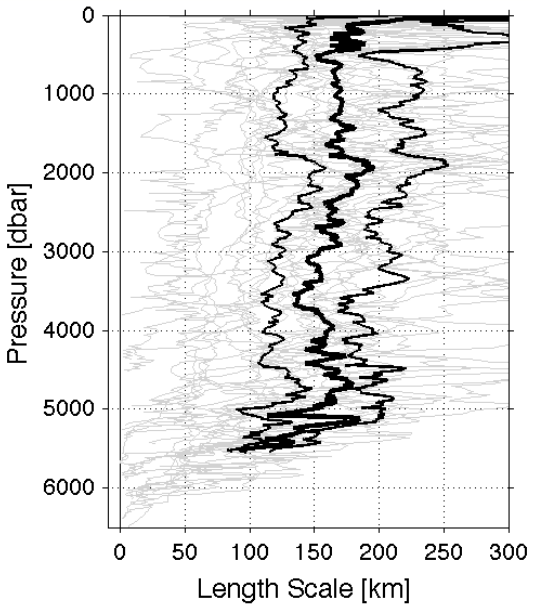

FIG. 6. Horizontal decorrelation length scales (km) of $d\theta/dt$ for each of the 26 repeat sections (gray lines) calculated at each pressure. The median (thick black line) and lower and upper interquartile range (thin black lines) are calculated from all sections with horizontal lengths greater than 2000 km at a given pressure. The pressure-averaged mean and median of length scale from 500–5000 dbar is 163 km.

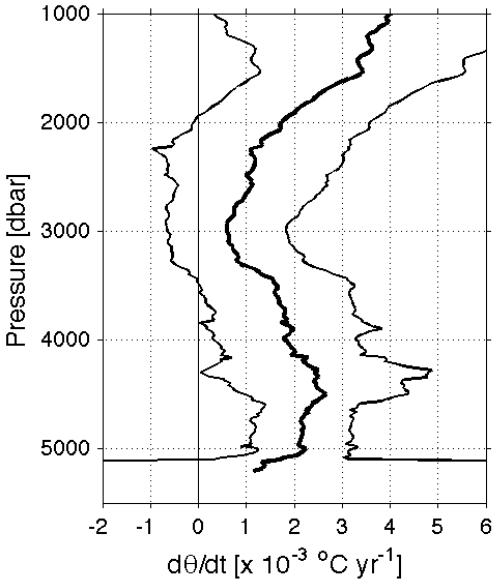

FIG. 7. Mean (thick black line) and 95% confidence limits (thin black lines) of $d\theta/dt$ for the Southeast Pacific Basin calculated as described in the text — a length-weighted combination of the portions of repeated sections (in this instance P18 and P16, see Fig. 1 for locations) that cross the basin.

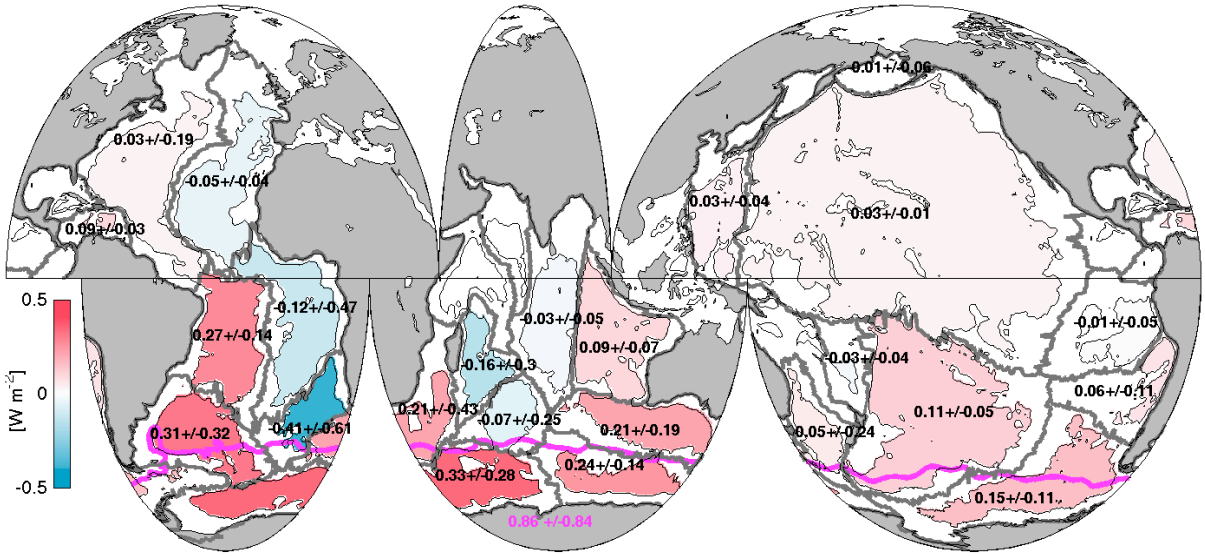

FIG. 8. Mean local heat fluxes through 4000 m implied by abyssal warming below 4000 m from the 1990s to the 2000s within each of the 24 sampled basins indicated by black numbers and color (see key), as well as 95% confidence intervals. Basin boundaries (thick gray lines) and 4000-m isobaths (thin grey lines) are shown. The local contribution to the heat flux through 1000 m south of the SAF (maroon line) implied by deep Southern Ocean warming from 1000–4000 m is also given (maroon number) with its 95% confidence interval.

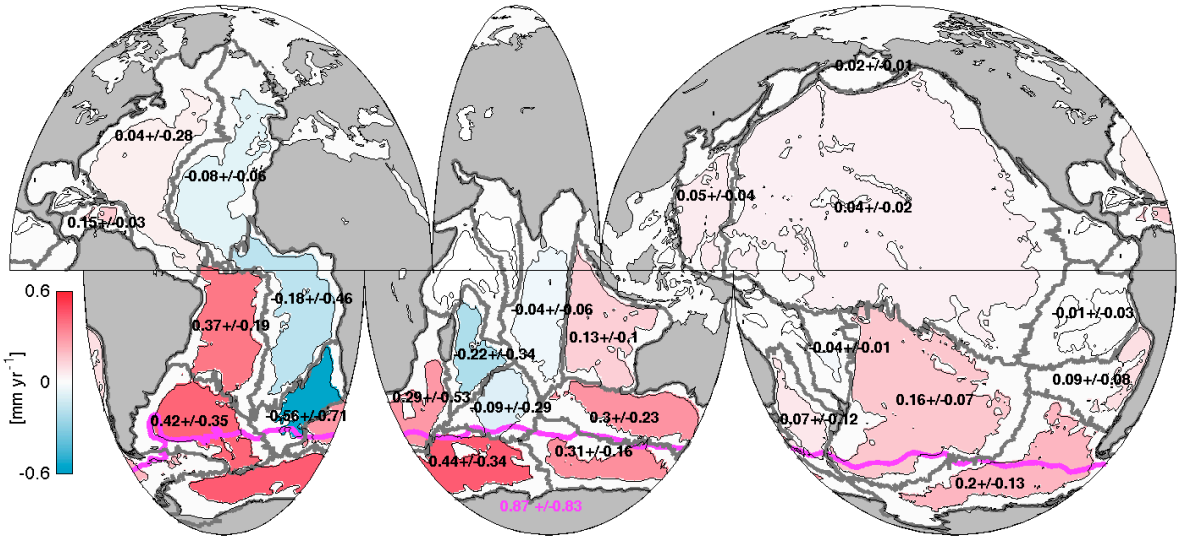

FIG. 9. Basin means of Sea Level Rise (SLR) from the 1990s to the 2000s due to abyssal thermal expansion below 4000 m and deep thermal expansion in the Southern Ocean from 1000–4000 m south of the SAF. Details follow Fig. 8.

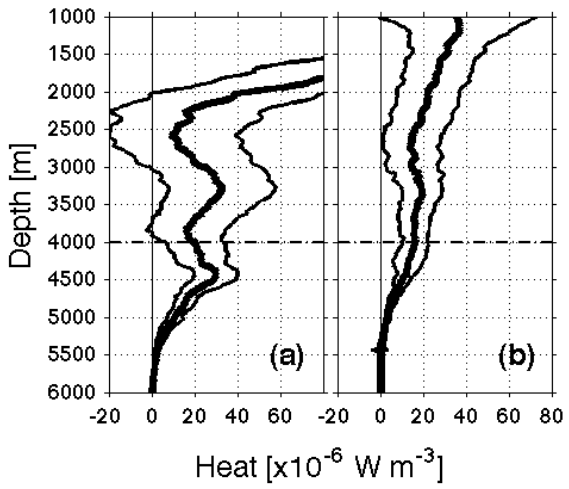

FIG. 10. Profiles of heat gain per meter (thick lines) with 95% confidence intervals (thin lines) estimated as described in (3) for (a) the global ocean and (b) the Southern Ocean south of the SAF.

Interface depth (m)	Heat (W m^{-2})			SLR (mm yr^{-1})		
	Global: below interface depth	**South of SAF: 1000-interface depth**	**Total**	**Global: below interface depth**	**South of SAF: 1000-interface depth**	**Total**
3000	0.049 (±0.034)	0.048 (±0.048)	0.097 (±0.059)	0.088 (±0.060)	0.060 (±0.062)	0.148 (±0.086)
4000	0.024 (±0.010)	0.065 (±0.063)	0.089 (±0.064)	0.047 (±0.020)	0.087 (±0.083)	0.134 (±0.086)

TABLE 1. Heat fluxes over the entire surface area of the earth required to explain the recent decadal observed temperature changes for the global ocean below the interface depth, the ocean south of the Sub Antarctic Front (SAF) between 1000 m and the interface depth, and the sum of the previous two terms. Similarly, mean sea level rise (SLR) over the global ocean due to the thermal expansion estimated from the recent decadal temperature changes observed in the three regions described above.